JOURNAL OF AIRCRAFT
Vol. 31, No. 4, July–Aug. 1994

Helicopter Rotor Lift Distributions for Minimum-Induced Power Loss

Steven R. Hall* and Kyle Y. Yang†
Massachusetts Institute of Technology, Cambridge, Massachusetts 02139
and
Kenneth C. Hall‡
Duke University, Durham, North Carolina 27706

A method is described for solving the minimum-induced loss (MIL) rotor design problem. First, the generalized Betz condition for MIL rotors is developed. Because the resulting lift distributions would generally exceed the maximum blade lift coefficient on the retreating side of the rotor, the necessary conditions are extended to include constraints on the lift. A method for solving for the optimum lift distribution using finite elements is described. Numerical results are presented for a typical rotor in forward flight. The MIL rotor may have on the order of 10% less induced power loss than a typical unoptimized rotor.

Nomenclature

A = rotor disk area, πR^2
a = blade section lift curve slope
B = matrix associated with force constraints
C = matrix associated with moment constraints
C_L = section lift coefficient
C_P = coefficient of power, $P/\rho A(\Omega R)^3$
C_T = thrust coefficient, $T/\rho A(\Omega R)^2$
c = blade chord
E = kinetic energy in wake
$\boldsymbol{F}$ = rotor force vector
G = matrix relating circulation to the potential
H = aft in-plane rotor force
$\hat{\imath}, \hat{\jmath}, \hat{k}$ = unit vectors in the aft, right, up directions
K = finite element matrix
L = lift produced by a single blade
$\boldsymbol{M}$ = vector of rotor moments
M_x = rotor hub rolling moment
M_y = rotor hub pitching moment
N = number of blades
$\hat{\boldsymbol{n}}$ = unit vector normal to surface
P_i = induced power
Q = rotor shaft torque
R = rotor radius
r = blade radial station
$\boldsymbol{r}$ = vector from hub center to blade station r
$\hat{\boldsymbol{r}}$ = unit vector along $\boldsymbol{r}$
$\bar{r}_c$ = nondimensional root cutout
S = surface of control volume V
T = rotor thrust
U = velocity of blade normal to blade axis
V = control volume
$\boldsymbol{V}$ = helicopter velocity vector
$\boldsymbol{v}$ = induced velocity in wake
W = wake sheet surface
w = induced velocity at rotor disk
x = coordinate axis, positive aft
Y = rotor in-plane side force
y = coordinate axis, positive to right
z = coordinate axis, positive up
γ = circulation Lagrange multiplier
$\boldsymbol{\gamma}$ = circulation Lagrange multiplier vector
Γ = circulation
$\boldsymbol{\Gamma}$ = vector of circulation at computational nodes
θ_{tw} = linear blade twist
κ = rotor-induced loss factor
λ = vertical advance ratio, $V_z/\Omega R$
μ = forward advance ratio, $-V_x/\Omega R$
$\boldsymbol{\nu}$ = vector of force Lagrange multipliers
ν_T = thrust Lagrange multiplier
$\boldsymbol{\xi}$ = Kelvin linear impulse
Π = induced power functional
ρ = density of air
σ = rotor solidity, $Nc/\pi R$
ϕ = potential function
ψ = azimuthal position on rotor disk
Ω = rotor rotational speed
$\boldsymbol{\Omega}$ = rotor rotation vector, $\Omega\hat{k}$
$\boldsymbol{\omega}$ = vector of moment Lagrange multipliers
ω_x = rolling moment Lagrange multiplier
ω_y = pitching moment Lagrange multiplier

Introduction

THE power required to drive the main rotor of a helicopter may be attributed to four sources: 1) profile power, 2) climb power, 3) parasite power, and 4) induced power. Of these, only the profile power and the induced power are directly affected by the design of the rotor. In this article, we consider how to achieve the minimum-induced power loss for a given forward flight condition by tailoring the lift distribution of the rotor.

It has long been recognized that tailoring the lift distribution of a rotor could improve performance. One method for changing the lift distribution is higher harmonic control (HHC) of blade pitch. Stewart[1] and Payne[2] considered the use of HHC to prevent the onset of blade stall on the retreating side, and compressibility losses on the advancing side. Stewart considered the use of 2/rev HHC. Payne extended this analysis to include both 2/rev and N/rev control. Stewart[1] concluded that by tailoring the lift distribution using 2/rev control, the max-

Received April 26, 1993; revision received Aug. 2, 1993; accepted for publication Aug. 4, 1993.

*Associate Professor, Department of Aeronautics and Astronautics. Associate Fellow AIAA.
†Research Assistant, Department of Aeronautics and Astronautics. Student Member AIAA.
‡Assistant Professor, Department of Mechanical Engineering and Materials Science. Member AIAA.

imum forward advance ratio (ratio of forward speed to tip speed) of a helicopter could be increased by as much as 0.1. Stewart also concluded that 2/rev control would have little beneficial effect on power requirements. Using more sophisticated performance prediction methods, Arcidiacono[3] predicted similar forward speed increases with 2/rev and 3/rev control, but also took the significant step of attempting to identify the characteristics of the ideal lift distribution to reduce retreating blade stall. His proposed ideal consisted of an azimuthally-discontinuous lift distribution with a slightly negative lift on the advancing side to counter moment imbalances. This effectively required much greater lifts toward the fore and aft regions of the lift distribution. Shaw et al.[4] conducted wind-tunnel tests that demonstrated potential performance benefits of 2/rev swashplate control. Using 2 deg of control input, phased pitch-up on the advancing and retreating blade areas, the power required was reduced by 6% at 135 kt and 4% at 160 kt on a Boeing CH-47D rotor. In an analytical study using comprehensive computer performance prediction methods, Nguyen and Chopra[5] determined that 2 deg of pitch input could reduce shaft power by up to 3.8% for the rotor under study.

Another way to change the lift distribution around the rotor disk is by the use of a controllable-twist rotor (CTR),[6] in which the blade root pitch is controlled by a conventional swashplate, and the blade twist is controlled by servotabs near the blade tips. The servotabs are actuated by a separate swashplate. Wind-tunnel tests of such a rotor and a conventional H-34 rotor suggested that the CTR could produce up to 20% more lift at some flight conditions by delaying blade stall, with negligible effects on the total power required.[7]

A more recent approach is to use multidisciplinary optimization (MDO) to optimize rotor performance.[8,9] In this approach, rotor parameters, such as blade planform, bending and torsional stiffness, and blade mass properties are allowed to vary. Using a comprehensive rotor analysis program, the rotor parameters are optimized to minimize power required, vibration, and hub loads.

One feature common to these three approaches is that, in each case, the lift distribution that can be achieved is limited by the technology of the rotor. An alternative approach is to use a smart rotor, which has enough actuation authority to allow tailoring of the lift distribution across the entire rotor disk. This may be accomplished, e.g., by using control surfaces distributed along the span of each blade. Spangler and Hall[10] have demonstrated the feasibility of piezoelectrically-actuated servoflaps, both analytically and in wind-tunnel tests. It has also been shown that these servoflaps should have enough control authority for other purposes, such as vibration control.[11] Therefore, distributed servoflaps appear to be a promising method for direct control of rotor aerodynamics. In particular, it should be possible to design a servoflap schedule to achieve a desired lift distribution across the rotor disk. Given the ability to control the lift distribution, it remains to determine the optimal distribution. The goal of this article, therefore, is to develop a method for determining minimum induced loss (MIL) rotor lift distributions.

The problem of determining MIL lift distributions for rotors is conceptually the same as the MIL propeller problem, for which analytical and semianalytical results exist. Betz[12] described the necessary conditions to achieve the minimum induced power loss at a given thrust and advance ratio for a lightly loaded propeller. Betz also solved the necessary conditions for the limiting case of a propeller with an infinite number of blades. Prandtl[13] found an approximate solution for a finite number of blades by adding a correction factor to account for tip effects. Goldstein[14] developed a numerical method for determining the exact solution for the problem by using infinite series to solve the elliptic partial differential equations that govern the flow between the vortex sheets of two adjacent blades. A summary of propeller theory is given by Glauert.[15] In an unpublished work, Munro[16] showed that Betz's optimality condition could be generalized to lightly loaded rotors.

In this article, the generalized Betz condition for MIL rotors in forward flight is presented. The condition is extended to include constraints, such as maximum blade section lift coefficient. A numerical method for solving the optimality conditions, based on finite elements, is described. Finally, examples of MIL rotor lift distributions are given, and compared to typical rotor lift distributions.

Calculation of Rotor Performance

In this section, two methods for determining the performance of a helicopter rotor are presented, near-wake analysis and far-wake analysis. In the near-wake theory, the induced power is viewed as a consequence of induced flow (downwash) at the rotor disk. The downwash at the rotor disk is a result of the trailing and shed vorticity in the rotor wake. In far wake theory, the induced power is equated with the rate at which kinetic energy is added to the rotor wake. This formulation requires that the structure of the wake be determined in the far wake, downstream of the rotor. Of course, the two theories are simply different ways of viewing the same problem, and so should give the same result.

Near-Wake Analysis

Most comprehensive rotor performance analyses are based on a near-wake analysis. Typically, the blade sectional lift is found using two-dimensional airfoil theory, using the fact that rotor blades have large aspect ratios. The bound circulation is then related to the sectional lift using lifting line theory. Finally, the trailing and shed vorticity in the wake are due to spanwise variations and time variations in the bound circulation, respectively. In this section, we assume that the lift distribution (or equivalently, the circulation) is given, and discuss how the rotor performance is determined.

The instantaneous lift on a single blade is given by

$$L = \int_0^R \rho\Gamma(\mu\Omega R \sin\psi + \Omega r)\, dr \tag{1}$$

where $\mu\Omega R \sin\psi + \Omega r$ is the component of the in-plane blade velocity normal to the blade section. The average thrust is then

$$T = \frac{N}{2\pi}\int_0^{2\pi}\int_0^R \rho\Gamma(\mu\Omega R \sin\psi + \Omega r)\, dr\, d\psi \tag{2}$$

The average aft force and side force are

$$H = \frac{N}{2\pi}\int_0^{2\pi}\int_0^R \rho\Gamma\lambda\Omega R \sin\psi\, dr\, d\psi \tag{3}$$

$$Y = -\frac{N}{2\pi}\int_0^{2\pi}\int_0^R \rho\Gamma\lambda\Omega R \cos\psi\, dr\, d\psi \tag{4}$$

The forces on the rotor may be expressed compactly in vector form as

$$\begin{aligned} \boldsymbol{F} &= H\hat{\imath} + Y\hat{\jmath} + T\hat{k} \\ &= \frac{N}{2\pi}\int_0^{2\pi}\int_0^R \rho\Gamma\hat{\boldsymbol{r}} \times (\boldsymbol{V} + \boldsymbol{\Omega} \times \boldsymbol{r})\, dr\, d\psi \end{aligned} \tag{5}$$

where $\boldsymbol{V}$ is the helicopter velocity vector

$$\boldsymbol{V} = (-\mu\hat{\imath} + \lambda\hat{k})\Omega R \tag{6}$$

Similarly, the rolling and pitching moments are

$$M_x = \frac{N}{2\pi}\int_0^{2\pi}\int_0^R \rho\Gamma(\mu\Omega R \sin\psi + \Omega r) r \sin\psi \, dr \, d\psi \quad (7)$$

$$M_y = -\frac{N}{2\pi}\int_0^{2\pi}\int_0^R \rho\Gamma(\mu\Omega R \sin\psi + \Omega r) r \cos\psi \, dr \, d\psi \quad (8)$$

The rotor shaft torque is

$$Q = \frac{N}{2\pi}\int_0^{2\pi}\int_0^R \rho\Gamma\lambda\Omega R r \, dr \, d\psi \quad (9)$$

The total moment on the rotor may be expressed in vector form as

$$\begin{aligned} \boldsymbol{M} &= M_x\hat{\imath} + M_y\hat{\jmath} - Q\hat{k} \\ &= \frac{N}{2\pi}\int_0^{2\pi}\int_0^R \rho\Gamma \boldsymbol{r} \times [\hat{\boldsymbol{r}} \times (\boldsymbol{V} + \boldsymbol{\Omega} \times \boldsymbol{r})] \, dr \, d\psi \end{aligned} \quad (10)$$

To compute the induced power, the induced velocities $w(r, \psi)$ must be determined at the rotor disk. The increment in induced power produced by each radial blade station is the incremental lift vector at the station dotted with the induced velocity. The average induced power is therefore

$$P_i = -\frac{N}{2\pi}\int_0^{2\pi}\int_0^R \rho\Gamma \boldsymbol{w} \cdot [\hat{\boldsymbol{r}} \times (\boldsymbol{V} + \boldsymbol{\Omega} \times \boldsymbol{r})] \, dr \, d\psi \quad (11)$$

A widely used method for determining the inflow (and hence, the induced power) at the rotor disk is the vortex lattice method. In this method, the vorticity in the wake sheet is modeled by discrete elements of trailing and shed vorticity. The strengths of the vortex elements are determined from the bound circulation $\Gamma(r, \psi)$. The contribution to the inflow from each vortex element is calculated using the Biot-Savart law.

There are several possible wake geometries that may be used. The geometry of a rigid wake is determined solely by the blade motion, without corrections for self-induced wake distortion. A prescribed wake incorporates the gross effects of the induced flow, perhaps using momentum theory. Finally, in a free wake analysis, the wake motion is based on the calculated induced flows. The first successful vortex lattice analyses used a rigid wake.[17] Since then, more sophisticated analyses have been developed using a free wake.[18]

One of the difficulties with vortex lattice methods is that the discretization of the wake into discrete vortex elements introduces singularities into the wake, producing unrealistically large velocities near the vortex elements. This results in the so-called encounter problem. Due to the geometry of the wake at high advance ratios, it is inevitable that some of the control points where the induced velocities are calculated will be very close to a vortex element, in which case the induced velocity calculated for that point will have a large error. Although this effect can be reduced somewhat by the introduction of a finite core radius, the induced velocity is strongly dependent on distance to a vortex segment. Because the errors introduced by the encounter problem are random, the effect is not too great for a given smooth lift distribution. However, these errors make the approach unsuitable for optimization purposes because the optimization would attempt to take advantage of the errors introduced due to the encounter problem.

Far-Wake Analysis

MIL propeller theory is based on the observation that thrust is a consequence of momentum in the wake, and induced power loss is a consequence of energy in the wake. Therefore, the thrust and power loss can be deduced from the structure of the wake, without any reference to how the wake was generated. Of course, the same is true for helicopter rotors. Munro,[16] in an unpublished report, determined how Betz's optimality condition could be extended to a lightly loaded rotor in forward flight. In this section, the theory for determining the performance of a lightly loaded rotor is developed, following Munro's theory.

Fig. 1 Geometry of a rotor wake.

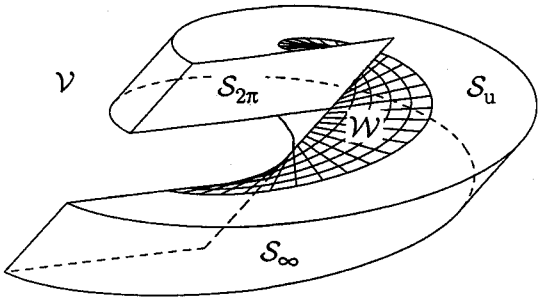

Fig. 2 Control volume V. The control volume is enclosed by the surface S, which is composed of the upper and lower surfaces S_u and S_l, the vertical surfaces S_0 and $S_{2\pi}$, and the outer bounding surface S_∞. The surfaces S_0 and S_l are hidden in the figure.

The key assumption required in the following development is the light loading assumption. For lightly loaded rotors, the induced velocities in the wake are small compared to the rotor velocity. This implies that the wake sheet left behind the rotor will be undistorted by the induced flows, at least for a considerable distance behind the rotor. As a result, the far wake will be undistorted and periodic. Hence, the light loading assumption is equivalent to the rigid wake assumption in vortex lattice methods. The geometry of the wake left behind a rotor is shown in Fig. 1.

Another assumption is that the induced flow in the wake is incompressible potential flow, with velocity potential ϕ. This assumption is valid even though the rotor blade tips are often transonic, since it is the induced velocities that are of concern here. A consequence of this assumption and the light loading assumption is that the induced flowfield and potential function are periodic in the far wake.

Because the far wake is periodic, the performance of the rotor can be determined from the flow in the volume V representing a single period of the wake (see Fig. 2). The forces on the rotor are proportional to the momentum in the volume; the induced power is proportional to the energy in the volume. The volume is enclosed by the surface S. The upper and lower surface of S, S_u, and S_l, are skewed helical surfaces that contain adjacent wake sheets. The upper wake sheet is labeled W. Note that the radius of V is infinite, so that the periodic far wake can be built up from an infinite number of similar control volumes, each displaced by the distance covered by the rotor in one blade-passage period. In essence, V is the volume enclosed by the wakes from two adjacent blades of the rotor as they sweep through one rotor revolution, if the blades are considered to be infinitely long.

The momentum in the wake is given by

$$\boldsymbol{\xi} = \int_V \rho\nabla\phi \, dV \quad (12)$$

Using the divergence theorem, the momentum may be rewritten in terms of the surface integral

$$\boldsymbol{\xi} = \int_S \rho\phi\hat{\boldsymbol{n}}\, dA \tag{13}$$

where $\hat{\boldsymbol{n}}$ is the unit outward normal on S. Note that ϕ is periodic, and ϕ is continuous, except across the wake sheet. Therefore, the potential function is equal on opposite sides of V(S_0 and $S_{2\pi}$, S_u, and S_l), except on the wake sheet itself, where the difference in the potentials is just the bound circulation Γ. Also, the unit normals are in opposite directions on opposite sides of V. Finally, $\phi = 0$ far away from the wake, and in particular on the outer bounding surface S_∞. Therefore, Eq. (13) reduces to

$$\boldsymbol{\xi} = -\int_W \rho\Gamma\hat{\boldsymbol{n}}\, dA \tag{14}$$

This may be recognized as the Kelvin linear impulse[19] generated by one turn of the wake sheet. The average force on the rotor is the negative of the impulse generated in one wake period, divided by the blade-passage period. Therefore

$$\boldsymbol{F} = -\frac{N\Omega}{2\pi}\boldsymbol{\xi} = \frac{N\Omega}{2\pi}\int_W \rho\Gamma\hat{\boldsymbol{n}}\, dA \tag{15}$$

Similarly, the average moment on the rotor is

$$\boldsymbol{M} = \frac{N\Omega}{2\pi}\int_W \rho\Gamma\boldsymbol{r}\times\hat{\boldsymbol{n}}\, dA \tag{16}$$

Equations (15) and (16) may be reconciled with Eqs. (5) and (10) by noting that

$$\Omega\hat{\boldsymbol{n}}\, dA = \hat{\boldsymbol{r}}\times(\boldsymbol{V} + \boldsymbol{\Omega}\times\boldsymbol{r})\, dr\, d\psi \tag{17}$$

To compute the induced power loss, we first determine the energy in one period of the wake. The kinetic energy in V is

$$E = \int_V \frac{\rho}{2}|v|^2\, dV = \int_V \frac{\rho}{2}|\nabla\phi|^2\, dV \tag{18}$$

The kinetic energy may be expressed in terms of the behavior at the wake sheet, so that

$$\begin{aligned} E &= \int_V \frac{\rho}{2}[\nabla\cdot(\phi\nabla\phi) - \phi\nabla^2\phi]\, dV \\ &= \int_S \frac{\rho}{2}\phi\nabla\phi\cdot\hat{\boldsymbol{n}}\, dA \\ &= -\int_W \frac{\rho}{2}\Gamma\boldsymbol{v}\cdot\hat{\boldsymbol{n}}\, dA \end{aligned} \tag{19}$$

where we have used the fact that $\nabla^2\phi = 0$ in the interior of V, applied the divergence theorem, and made simplifications similar to those made to obtain Eq. (15). Therefore, the time-averaged induced power is given by

$$P_i = -\frac{N\Omega}{2\pi}\int_W \frac{\rho}{2}\Gamma\boldsymbol{v}\cdot\hat{\boldsymbol{n}}\, dA \tag{20}$$

The induced power found using the near wake theory [Eq. (11)] may be rewritten as

$$P_i = -\frac{N\Omega}{2\pi}\int_W \rho\Gamma\boldsymbol{w}\cdot\hat{\boldsymbol{n}}\, dA \tag{21}$$

In both Eqs. (20) and (21), the induced power depends on the product of the induced flow ($\boldsymbol{w}$ or $\boldsymbol{v}$) and the bound vorticity, integrated over the area of the wake. In Eq. (20), the induced flow is the induced flow in the far wake, whereas in Eq. (21), the induced flow is at the rotor disk. A similar result holds for the fixed-wing and propeller cases. In those cases, $v = 2w$, which accounts for the factor of two difference in the equations. However, it is not true that $v = 2w$ for a rotor, because the symmetry that exists for wings and propellers is lost, due to the skewed geometry of a rotor wake.

As a practical matter, the applicability of the far-wake analysis may seem to be limited by the assumption of light loading. However, experiments on hovering rotors (which are not lightly loaded) have indicated that the theories are robust.[20] In these experiments, a two-bladed rotor operating at blade loadings C_T/σ ranging from 0.04 to 0.11 was shown to have power requirements that closely matched those predicted by Goldstein's theory.

Optimality Conditions

In this section the optimality conditions for a minimum induced loss rotor are derived, based on the far-wake theory of the previous section. The optimality conditions have a geometrical interpretation similar to the interpretations given for the wing and propeller cases. Also, it will be shown that there is a natural variational principle that describes the MIL solution. This variational principle will prove useful for developing numerical optimization techniques.

The goal is to find the rotor lift distribution that minimizes the induced power loss subject to the constraint that the rotor is in trim, i.e., has the required thrust, rolling moment, and pitching moment. Additional constraints may be required to ensure that the sectional blade loading is not physically unrealizable, especially near the root and on the retreating side. We first describe the case where the sectional lift, or equivalently, the circulation, is unconstrained.

Unconstrained Circulation

The derivation of the unconstrained optimum again follows Munro's theory.[16] To optimize the performance of the rotor, the induced power can be augmented with the trim constraints using Lagrange multipliers to form the induced power functional

$$\begin{aligned} \Pi &= P_i + \nu_T(T - T_{\text{req}}) \\ &\quad + \omega_x(M_x - M_{x_{\text{req}}}) + \omega_y(M_y - M_{y_{\text{req}}}) \\ &= P_i + \boldsymbol{\nu}\cdot(\boldsymbol{F} - \boldsymbol{F}_{\text{req}}) + \boldsymbol{\omega}\cdot(\boldsymbol{M} - \boldsymbol{M}_{\text{req}}) \end{aligned} \tag{22}$$

where $(\,)_{\text{req}}$ denotes the required force or moment, and

$$\boldsymbol{\nu} = \nu_T\hat{\boldsymbol{k}} \tag{23}$$

$$\boldsymbol{\omega} = \omega_x\hat{\boldsymbol{i}} + \omega_y\hat{\boldsymbol{j}} \tag{24}$$

The induced power functional can be expanded in terms of Eqs. (15), (16), and (18), so that

$$\begin{aligned} \Pi &= \frac{N\Omega}{2\pi}\int_V \frac{\rho}{2}|\nabla\phi|^2\, dV \\ &\quad + \frac{N\Omega}{2\pi}\int_W \rho\Gamma[\boldsymbol{\nu}\cdot\hat{\boldsymbol{n}} + \boldsymbol{\omega}\cdot(\boldsymbol{r}\times\hat{\boldsymbol{n}})]\, dA \\ &\quad - \nu_T T_{\text{req}} - \omega_x M_{x_{\text{req}}} - \omega_y M_{y_{\text{req}}} \end{aligned} \tag{25}$$

The variation of the induced power functional is easily determined, except for the first term. Its variation is given by

$$\begin{aligned}\delta P_i &= \frac{N\Omega}{2\pi}\int_V \rho\nabla\delta\phi\cdot\nabla\phi\ dV \\ &= \frac{N\Omega}{2\pi}\int_V \rho(\nabla\cdot(\delta\phi\nabla\phi) - \delta\phi\nabla^2\phi)\ dV \\ &= \frac{N\Omega}{2\pi}\int_S \rho\delta\phi\nabla\phi\cdot\hat{\boldsymbol{n}}\ dA - \frac{N\Omega}{2\pi}\int_V \rho(\nabla^2\phi)\delta\phi\ dV \\ &= -\frac{N\Omega}{2\pi}\int_W \rho v\cdot\hat{\boldsymbol{n}}\delta\Gamma\ dA - \frac{N\Omega}{2\pi}\int_V \rho(\nabla^2\phi)\delta\phi\ dV\end{aligned} \tag{26}$$

Therefore, the variation of the induced power functional is given by

$$\begin{aligned}\delta\Pi = &\frac{N\Omega}{2\pi}\int_W \rho(\boldsymbol{\nu}\cdot\hat{\boldsymbol{n}} + \boldsymbol{\omega}\cdot(\boldsymbol{r}\times\hat{\boldsymbol{n}}) - v\cdot\hat{\boldsymbol{n}})\delta\Gamma\ dA \\ &- \frac{N\Omega}{2\pi}\int_V \rho(\nabla^2\phi)\delta\phi\ dV + \delta\nu_T(T - T_{\text{req}}) \\ &+ \delta\omega_x(M_x - M_{x_{\text{req}}}) + \delta\omega_y(M_y - M_{y_{\text{req}}})\end{aligned} \tag{27}$$

The first-order necessary condition for the lift distribution to be optimal is that $\delta\Pi = 0$ for all allowable perturbations. Therefore, the optimality conditions are

$$T = T_{\text{req}} \tag{28}$$

$$M_x = M_{x_{\text{req}}} \tag{29}$$

$$M_y = M_{y_{\text{req}}} \tag{30}$$

$$(\nabla^2\phi)\delta\phi = 0 \tag{31}$$

$$v\cdot\hat{\boldsymbol{n}} = (\boldsymbol{\nu} + \boldsymbol{\omega}\times\boldsymbol{r})\cdot\hat{\boldsymbol{n}} \tag{32}$$

Conditions (28–30) are simply the trim conditions. Condition (31) is automatically satisfied for any potential flow, since $\nabla^2\phi = 0$. Condition (32) has a geometrical interpretation. The optimum vorticity distribution in the wake is the same as that produced by the flow past an impermeable membrane (the wake sheet) which translates at speed $\boldsymbol{\nu}$ and shears at angular rate $\boldsymbol{\omega}$. The shearing results (rather than a rigid rotation) because the rotation occurs about the point in the wake corresponding to the hub location at the time the wake element was generated. These conditions are similar to Betz's rigid wake condition for MIL propellers.

Constrained Circulation

The derivation above places no constraints on the blade section lift coefficient (and therefore, the circulation). In practice, this will lead to lift coefficients that exceed the maximum sectional lift coefficient of the blade, particularly on the retreating side of the rotor. Therefore, the analysis of the previous section will be extended to incorporate constraints on the lift.

Γ may be related to the blade C_L by

$$\Gamma = \tfrac{1}{2}|U|cC_L \tag{33}$$

where U is the sectional velocity, i.e., the velocity of the blade normal to the blade axis. Therefore, the constraint on the circulation is given by

$$\Gamma \le \Gamma_{\max} = \tfrac{1}{2}|U|cC_{L_{\max}} \tag{34}$$

To impose this condition, the constraint is added to the induced power functional with γ, so that

$$\begin{aligned}\Pi = &P_i + \boldsymbol{\nu}\cdot(\boldsymbol{F} - \boldsymbol{F}_{\text{req}}) + \boldsymbol{\omega}\cdot(\boldsymbol{M} - \boldsymbol{M}_{\text{req}}) \\ &+ \frac{N\Omega}{2\pi}\int_W \gamma(\Gamma - \Gamma_{\max})\ dA\end{aligned} \tag{35}$$

The variation in the induced power functional is then

$$\begin{aligned}\delta\Pi = &\frac{N\Omega}{2\pi}\int_W \rho(\boldsymbol{\nu}\cdot\hat{\boldsymbol{n}} + \boldsymbol{\omega}\cdot(\boldsymbol{r}\times\hat{\boldsymbol{n}}) + \gamma - v\cdot\hat{\boldsymbol{n}})\ \delta\Gamma\ dA \\ &+ \frac{N\Omega}{2\pi}\int_W (\Gamma - \Gamma_{\max})\delta\gamma\ dA \\ &- \frac{N\Omega}{2\pi}\int_V \rho(\nabla^2\phi)\delta\phi\ dV + \delta\nu_T(T - T_{\text{req}}) \\ &+ \delta\omega_x(M_x - M_{x_{\text{req}}}) + \delta\omega_y(M_y - M_{y_{\text{req}}})\end{aligned} \tag{36}$$

The necessary conditions are then Eqs. (28–31), and

$$\begin{cases}\gamma \ge 0, & \text{if } \Gamma = \Gamma_{\max} \\ \gamma = 0, & \text{if } \Gamma < \Gamma_{\max}\end{cases} \tag{37}$$

$$v\cdot\hat{\boldsymbol{n}} = (\boldsymbol{\nu} + \boldsymbol{\omega}\times\boldsymbol{r})\cdot\hat{\boldsymbol{n}} + \gamma \tag{38}$$

Conditions (37) and (38) also have a geometrical interpretation, although more complicated than in the unconstrained circulation case. The vorticity in the wake is the same as that of a potential flow past an impermeable membrane. In the region where $\Gamma < \Gamma_{\max}$, the membrane is moving with velocity $\boldsymbol{\nu}$ and shearing with angular rate $\boldsymbol{\omega}$. In the region where $\Gamma = \Gamma_{\max}$, the normal velocity of the membrane is reduced ($v\cdot\hat{\boldsymbol{n}} < 0$ except in the reverse flow region for positive thrust) by the velocity γ.

In both the unconstrained and constrained circulation cases, care should be exercised when interpreting the geometrical conditions. The potential function that results due to the wake vorticity is the same as that which results from the motion of an impermeable membrane. That does not imply that the wake moves rigidly with the same motion as the membrane, because the necessary condition constrains the normal component of the wake velocity, but not the tangential components. The wake will appear to move rigidly, but in fact may have tangential motion. See Ref. 21 for a discussion of this result in the propeller case.

Finally, note that it should be possible to add a term to the induced loss functional to account for the profile drag, since the profile drag is a function of the blade angle of attack, and the angle of attack determines the circulation.

Numerical Solution Procedure

One of the necessary conditions for the MIL rotor is that $\nabla^2\phi = 0$ in the interior of V, i.e., between the wake sheets. This condition is assumed a priori, but in fact is a necessary condition for the induced power functional to be stationary with respect to variations in ϕ. Because the optimal flow is described by a variational principle, the optimization problem may be discretized and solved using finite element techniques. In this section, the numerical procedure that results from such a procedure is described.

To discretize the problem, the domain V is divided into finite elements. The potential function ϕ is determined within each finite element by the value of the potential at the nodes of the element using interpolation functions. The induced power functional [Eq. (25)] is then numerically integrated to yield the discrete induced power functional

$$\Pi_d = \tfrac{1}{2}\boldsymbol{\phi}^T K\boldsymbol{\phi} + \boldsymbol{\nu}^T(B\boldsymbol{\phi} - \boldsymbol{F}_{\text{req}}) + \boldsymbol{\omega}^T(C\boldsymbol{\phi} - \boldsymbol{M}_{\text{req}}) \tag{39}$$

where ϕ is the vector of unknown velocity potentials at the nodes of the elements. The matrix K is a large but sparse stiffness matrix that describes Laplace's equation within the computational domain. The matrices B and C are smaller matrices that are associated with the trim constraints. Setting the variation of Eq. (39) to 0 results in the linear Euler-Lagrange equation

$$\begin{bmatrix} K & B^T & C^T \\ B & 0 & 0 \\ C & 0 & 0 \end{bmatrix} \begin{Bmatrix} \phi \\ \nu \\ \omega \end{Bmatrix} = \begin{Bmatrix} 0 \\ F_{req} \\ M_{req} \end{Bmatrix} \tag{40}$$

For the case where the maximum lift coefficient is not constrained, the potential is found by solving the above sparse set of linear equations.

If, after solving Eq. (40), the maximum lift constraints are violated, constraints are added to those points on the rotor wake where Γ has exceeded Γ_{max}. Because of the nonlinear nature of these constraints, they cannot be added to the induced power functional in the same way as the linear constraints. We make use of the method of constrained optimization via augmented Lagrangians[22] to impose these constraints. If the constraint is in effect, then a quadratic penalty is added to the induced power functional that penalizes the difference between Γ and Γ_{max}. In addition, a Lagrange multiplier γ is introduced so that

$$\Pi_d = \tfrac{1}{2}\phi^T K\phi + \nu^T(B\phi - F_{req}) + \omega^T(C\phi - M_{req}) + \gamma^T(\Gamma - \Gamma_{max}) + \tfrac{1}{2}(\Gamma - \Gamma_{max})^T W(\Gamma - \Gamma_{max}) \tag{41}$$

where W is a diagonal matrix with large positive entries, Γ is the vector containing the circulation at each of the actively constrained nodes of the wake, and Γ_{max} is the corresponding vector of maximum circulations.

Note that the circulation at the actively constrained nodes may be expressed in terms of the potential as

$$\Gamma = G\phi \tag{42}$$

where G is a linear operator which computes the jump in potential across the wake at the constrained nodes. Combining Eqs. (41) and (42), taking the variation and setting the result to 0 results in the matrix equation

$$\begin{bmatrix} [K + G^T W G] & B^T & C^T \\ B & 0 & 0 \\ C & 0 & 0 \end{bmatrix} \begin{Bmatrix} \phi \\ \nu \\ \omega \end{Bmatrix} = \begin{Bmatrix} G^T W \Gamma_{max} - G^T \gamma \\ F_{req} \\ M_{req} \end{Bmatrix} \tag{43}$$

Equation (43) is solved for ϕ, ν, and ω. If W is large, then the constraint (42) will be very nearly satisfied. Furthermore, the actual Lagrange multiplier may be estimated using

$$\gamma_{new} = \gamma_{old} + W(\Gamma - \Gamma_{max}) \tag{44}$$

Having a new estimate for the Lagrange multipliers γ, one can then decide whether a constraint should be kept on the active constraint list or removed. If $\gamma_i > 0$, then the constraint is kept active. Conversely, if $\gamma_i < 0$, then the constraint should not be active, and the constraint is removed from the active list. Finally, it is possible that other computational nodes on the wake that are not currently on the active constraint list may now violate the maximum lift constraint. Each such node is added to the constraint list and a first estimate for the Lagrange multiplier is selected (usually zero). Equation (43) is then reassembled using the updated constraint list and Lagrange multipliers, and the entire process repeated until convergence is reached. Typically, only about 3–4 iterations are required to achieve satisfactory convergence.

Once the optimal flowfield has been computed, the induced power may be computed. This may be done in one of several ways. One may compute the power directly from the kinetic energy of the flow in the field, using

$$P_i = \tfrac{1}{2}\phi^T K\phi \tag{45}$$

The advantage to this technique is that the stiffness matrix K is readily available as a by-product of the optimization procedure. The disadvantage of this approach is that the computational domain is necessarily finite in extent. Hence, the volume integral may not be approximated well by this expression. Also, by the nature of the finite element method, the resulting induced power estimate will approach the exact answer from above (the estimate of the power is too high) as the grid is refined.

Alternatively, one could use the Γ distribution on the wake predicted by the present analysis, and then use a vortex lattice code to predict the induced wash normal to the wake. Then, a numerical integration of Eq. (11) may be carried out to predict the induced power. This approach may be more accurate than the field approach above, since the estimate for Γ is probably better than the estimate of the velocity field. Both methods have been used to calculate the induced power. Generally, the field method produces a slightly higher estimate of the induced power, a result that is consistent with the fact that the energy in the flow as predicted by a finite element method will in general be slightly too high.

For simplicity, linear, isoparametric, hexahedral elements are used throughout the computational domain. They are arranged in a logically rectangular array so that periodicity in the flow along the flight direction may be easily imposed. One drawback of the hexahedral meshing is that for large forward advance ratios of interest, the computational cells may be highly skewed. Furthermore, if the grid is generated so that it extends outward from the rotor roughly parallel to the plane of rotation, then the resolution will become increasingly poor downstream of the single turn of the wake. This creates a problem since the helical wake will pass close above or below the grid upstream and downstream of the turn in the wake. The close proximity of adjacent turns in the wake produces large gradients in the flow that cannot be adequately resolved with a coarse mesh. This latter problem may be alleviated somewhat by angling the grid normal to the velocity vector of the rotor for that portion of the grid outside the rotor radius. However, the problem of grid skew can be resolved only through the use of unstructured grid techniques.

The main benefit in using finite elements is that the resulting representation of the bound vorticity is piecewise linear along the span of the blade and in azimuthal position. Therefore, the trailing and shed vorticity is distributed smoothly in the wake sheet. On the other hand, the bound vorticity is piecewise constant for the vortex lattice method, resulting in discrete vortex elements in the wake sheet, and the resulting encounter problem.

Results

In this section, sample optimal loading calculations are presented for the case of a rotor in axial flight and a rotor in forward flight.

Axial Flight

The theory presented in this article applies to the special case of a rotor in axial flight, i.e., a propeller. Therefore, the present theory may be compared to Goldstein's propeller theory,[14] which is a numerical method for determining the optimal lift distribution on a propeller.

The case considered here is a four-bladed rotor in axial flight with vertical advance ratio $\lambda = 0.0775$. Shown in Fig. 3 is the optimal circulation distribution computed using the present theory. These results were computed using two dif-

Table 1 Induced power requirements for rotor in vertical flight; $N = 4$, $\lambda = 0.0775$

	κ		
Grid size	Finite element	Vortex lattice	Goldstein
77 × 61 × 29	1.086	1.067	1.067
39 × 31 × 15	1.077	1.067	1.067

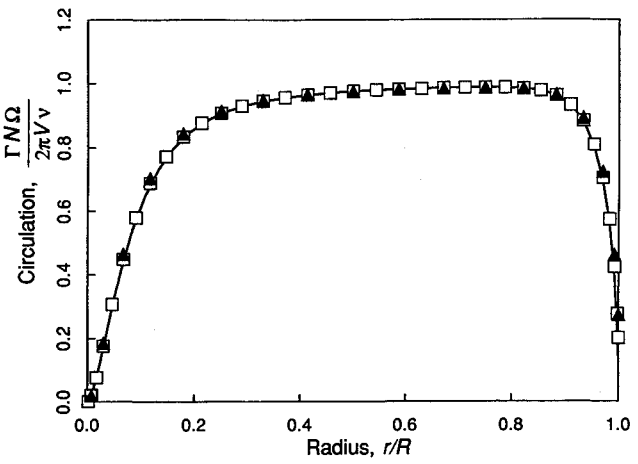

Fig. 3 Optimal bound circulation distribution for rotor in vertical climb. $N = 4$, $\lambda = 0.0775$. Goldstein theory, ——; present theory using a 39 × 31 × 15 computational grid, ▲; present theory using a 77 × 61 × 29 computational grid, □.

ferent grid resolutions (39 radial × 31 azimuthal × 15 axial and 77 × 61 × 29 node grids). Also shown for comparison is the solution found using Goldstein's method. Note the excellent agreement between the Goldstein result and the present analysis, even for the coarse grid calculation.

From momentum theory, the induced power for a lightly loaded actuator disk (without swirl or tip loss) is given by

$$C_P/C_T^2 = 1/(2\lambda) \tag{46}$$

Therefore, the loss factor κ is defined by

$$\kappa = 2\lambda(C_P/C_T^2) \tag{47}$$

In general, the loss factor must be greater than unity.

Using the computed optimal solutions, the induced power was computed in two different ways. First, the power was computed using the kinetic energy in the flowfield [Eq. (45)]. Second, the power was computed using the near-wake approach [Eq. (11)]. These results are given in Table 1. The induced normal wash was computed with a vortex lattice using the optimal Γ distribution to define the strength of the vortex elements. Finally, the results are compared to the Goldstein results. All three methods agree to within about 2%, with the variation probably due to the fact that the finite elements are slightly stiff, and therefore overestimate the power slightly. Somewhat surprisingly, the induced power for the fine grid case is slightly higher than in the coarse grid case, probably because the solution found using the iterative sparse matrix solver was not completely converged. In any case, the agreement in the circulation distribution is excellent.

Forward Flight

In this section, the more complicated case of a rotor in forward flight is considered. The case examined in this section was chosen to match an example presented in some detail by Johnson (Ref. 23, Chap. 13). Johnson performed the direct analysis problem of a typical rotor in forward flight. The parameters for this case are presented in Table 2.

Table 2 Parameters used for forward flight example

Thrust coefficient	C_T	0.012
Forward advance ratio	μ	0.25
Vertical advance ratio	λ	0.01
Number of blades	N	3
Rotor solidity	σ	0.1
Root cutout	$\bar{r}_c$	0.15
Linear blade twist	θ_{tw}	−8.0 deg
Nondimensional helicopter drag	f/A	0.015
Lock number	γ	8
Blade section lift curve slope	a	5.7

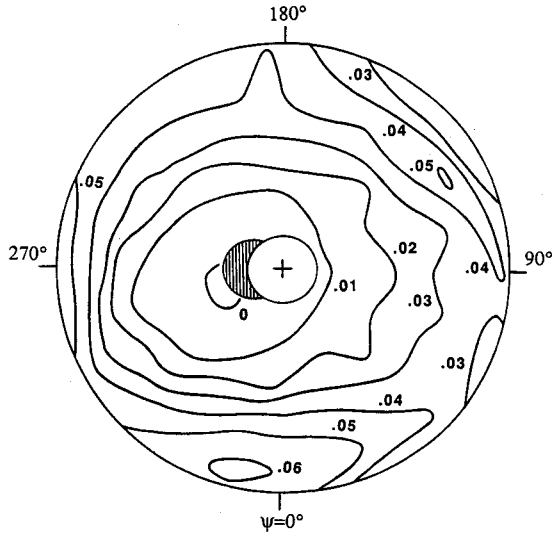

Fig. 4 Lift distribution for baseline rotor (from Ref. 23, p. 722). Plotted are contours of constant blade sectional lift, $l/\rho ac(\Omega R)^2$. Rotor parameters are given in Table 2. Shaded region indicates reverse flow.

Baseline Lift Distribution

Figure 4 shows the computed lift distribution for the baseline case. The lift distribution was determined using a prescribed wake vortex lattice analysis with an undistorted wake geometry (Ref. 23, p. 720). It should be emphasized that this is not an optimal lift distribution, but rather a typical unoptimized result. Although not apparent in the figure, there is a region of blade stall in the third quadrant near the reverse flow region. Also, note that in the figure, the lift does not roll off to zero at the tips, as must always occur for real blades. This is probably due to the fact that wake was modeled with a finite strength vortex at the tip, with a finite core radius. Generally, finite induced power lift distributions must have lift that rolls off as $\sqrt{(R - r)}$ near the tips.

Optimal Lift Distributions

Next, the optimal lift distribution for this case was computed using the present method with no constraint on the coefficient of lift ($C_{L\max} = \infty$). The rotor was constrained to have no pitching or rolling moments. The vertical advance ratio used to prescribe the geometry of the wake was set to $\lambda_{pre} = 0.034$ to account for the gross effects of momentum ($\lambda = 0.024$) and the tilt of the rotor disk ($\lambda = 0.01$). The computed optimal lift distribution is shown in Fig. 5. Several interesting features of the optimal lift distribution are observed. First, the optimal lift distribution rolls off at the tip with the expected square-root behavior. Hence, a finite strength tip vortex will not exist, but rather there will be a continuous vortex sheet. Second, away from the tip, the lift distribution is somewhat smoother than in the baseline case, indicating that much of the shed vorticity has been eliminated. Physically, less shed vorticity implies less unsteadiness in the flow and, therefore, lower induced power. Third, the optimal lift distribution is seen to be symmetric fore and aft.

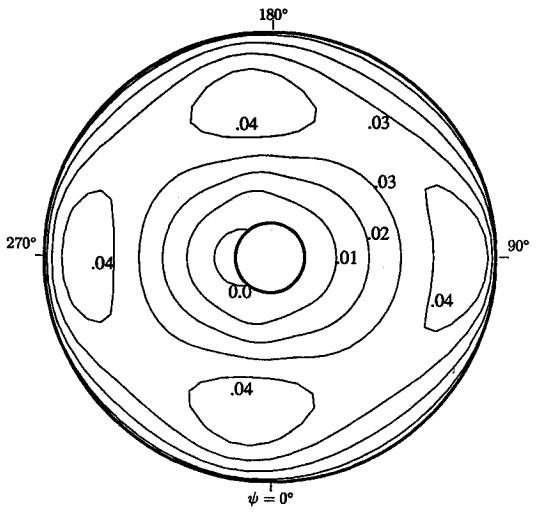

Fig. 5 Optimal lift distribution for rotor in forward flight. Plotted are contours of constant blade sectional lift, $l/\rho ac(\Omega R)^2$. Rotor parameters are given in Table 2.

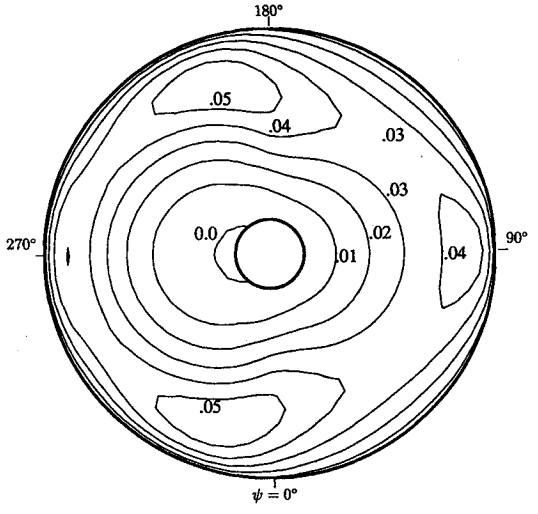

Fig. 6 Optimal lift distribution for rotor in forward flight with $C_{L\max}$ = 1.5. Plotted are contours of constant blade sectional lift, $l/\rho ac(\Omega R)^2$. Rotor parameters are given in Table 2.

It is not immediately obvious that the optimal lift should be symmetric fore and aft, even though the pitching moment is constrained to be zero. The reason the circulation (and hence, the lift) is symmetric can be understood by looking at the far wake. In the far-wake region, the wake is essentially symmetric in the flight direction. That is, the wake is symmetric with respect to a 180-deg rotation about the y axis. The symmetry in the wake geometry implies symmetry in the vorticity distribution when $\omega_y = 0$, as is the case here. The induced flow in the wake is also symmetric. This symmetry does not apply to the near wake, however. At the rotor disk, the optimal solution dictates a lift distribution that is symmetric fore and aft, but a nonsymmetric induced velocity field.

Next, consider the case where the blade sectional coefficient of lift is constrained not to exceed 1.5, which is the approximate maximum for an NACA 0012 airfoil.[24] The resulting lift distribution is shown in Fig. 6. Note the region on the retreating side where the lift constraint is in effect. In this region, the lift contours are sectors of concentric circles. Again, the lift is symmetric fore and aft. However, the largest lift is now concentrated fore and aft (cf. Fig. 5). The $C_{L\max}$ constraint limits the amount of lift that can be produced on the retreating side of the rotor. The trim constraints in turn limit the amount of lift that may be produced on the advancing side. The optimality condition tends to produce smooth lift distributions so as to reduce the unsteadiness in the flow. Hence, the lift is concentrated fore and aft, specifically at ψ = 200 and 340 deg. These observations are consistent with the observations of Nguyen and Chopra.[5] Nguyen and Chopra optimized the performance of a rotor which incorporated 2/rev control. They found that the optimal performance occurred when the pitch angle of the blades, and hence the lift, was increased toward the fore and aft regions.

Induced Power Requirements

In this section, induced power calculations are presented for the baseline and optimized rotors. To determine a figure of merit for each case, note that the induced power in forward flight is bounded by the fixed wing limit

$$C_P/C_T^2 \geq 1/(2\mu) \tag{48}$$

Therefore, κ is defined by

$$\kappa = 2\mu(C_P/C_T^2) \tag{49}$$

κ = 1 corresponds to the fixed-wing limit. The loss factor is always greater than unity because the optimal lift distribution is not elliptical in general, and there are additional sources of loss such as swirl, tip loss, and unsteadiness.

Two methods were used to compare the induced power for each case. As in the axial flight example, the power was computed using the near-wake analysis [Eq. (11)] with a vortex lattice code, and the far-wake analysis [Eq. (45)] with the finite element code.

One note on the power calculation of the baseline lift distribution is in order. As discussed earlier, the data for the baseline case indicates that the lift is finite at the tips. Computing the induced power using the baseline lift distribution without taking into account the finite tip core radius will result in estimates of the induced power that are too high. Therefore, the baseline lift distribution was optimized over the inner and outer 5% of the blades using the present analysis, while constraining the remainder of the lift to be unchanged. This has the effect of producing more reasonable induced power contributions from the tip vortices. Another benefit of this procedure is that the velocity potential is calculated in the field, and thus Eq. (45) may be used to compute the induced power for the baseline case.

The rotor induced loss factor for the baseline rotor and several optimal rotors is presented in Table 3. The table shows the rotor loss factor computed using the finite element method and the vortex lattice method. The finite element method and the vortex lattice method generally agree well, with about 1–2% variation in the calculation of the induced power for each case. The rotor loss factor is seen to be about 22–24% smaller for the unconstrained optimal rotor case than the baseline rotor case. As the maximum allowable coefficient of lift is lowered, the induced power increases. For the case $C_{L\max}$ = 1.5 (which is the approximate maximum lift coefficient in the baseline case), the optimum rotor induced loss is about 14% lower than the baseline case. Finally, for the case $C_{L\max}$ = 1.2, the induced loss is about the same as the baseline case. Thus, the performance of the minimum induced loss rotor

Table 3 Induced power requirements for rotor in forward flight

	Grid size	$C_{L\max}$	κ	
			Finite element	Vortex lattice
Baseline	——	——	1.75[a]	1.70[a]
Optimal	77 × 61 × 29	∞	1.32	1.33
Optimal	77 × 61 × 29	1.5	1.47	1.51
Optimal	77 × 61 × 29	1.2	1.68	1.72

[a]Original baseline lift distribution was optimized from 95% span outwards to minimize tip losses artificially induced from the discretization of the figure.

depends strongly on $C_{L\max}$, as might be expected. However, it appears that the induced losses may be significantly reduced on a typical rotor, if the lift distribution can be tailored as desired.

Concluding Remarks

In this article, a method was developed for determining rotor lift distributions subject to realistic constraints. The necessary conditions for the MIL rotor were found, and a geometric interpretation for these conditions was given. It was shown that the optimality conditions yield a variational principle for the optimization problem, suggesting the use of finite elements. A numerical method based on finite elements was developed. One desirable feature of the method is that the calculated power is an upper bound on the actual power for the given loading, at least in the light loading case. One difficulty with the numerical procedure is that the finite elements may be stiff, due to the high skew in the wake. An unstructured mesh technique may be used to solve this problem.

The method was demonstrated for a typical rotor. The results suggest that typical rotors have 10–15% more induced losses than the minimum induced loss rotor.

Acknowledgments

The first two authors were supported by a grant from NASA, NAG1-1299, funded by the Aeroperformance Division of the U.S. Army Aeroflightdynamics Directorate, with John Berry serving as technical monitor. The second author was supported primarily by a National Science Foundation Graduate Research Fellowship. The third author was supported through a curriculum development grant provided by the General Electric Foundation. Some calculations in this article were performed on the MIT Cray X-MP. Also, the authors would like to thank John Berry, Ken Powell and John Taylor of the University of Michigan, and Mark Drela of MIT for their helpful suggestions. Mark Drela also supplied the computer code for the Goldstein propeller calculations.

References

[1]Stewart, W., "Second Harmonic Control on the Helicopter Rotor," Aeronautical Research Council, R&M 2997, London, Aug. 1952.

[2]Payne, P. R., "Higher Harmonic Rotor Control," *Aircraft Engineering*, Vol. 30, No. 354, 1958, pp. 222–226.

[3]Arcidiacono, P. J., "Theoretical Performance of Helicopters Having Second and Higher Harmonic Feathering Control," *Journal of the American Helicopter Society*, Vol. 6, No. 2, 1961, pp. 8–19.

[4]Shaw, J., Albion, N., Hanker, E. J., Jr., and Teal, R. S., "Higher Harmonic Control: Wind Tunnel Demonstration of Fully Effective Vibratory Hub Force Suppression," *Journal of the American Helicopter Society*, Vol. 34, No. 1, 1989, pp. 14–25.

[5]Nguyen, K., and Chopra, I., "Effects of Higher Harmonic Control on Rotor Performance and Control Loads," *Journal of Aircraft*, Vol. 29, No. 3, 1992, pp. 336–342.

[6]McCloud, J. L., III, "An Analytical Study of a Multicyclic Controllable Twist Rotor," 31st Annual Forum, American Helicopter Society, Washington, DC, May 1975.

[7]Lemnios, A., "Full Scale Wind Tunnel Tests of a Controllable Twist Rotor," 32nd Annual Forum, American Helicopter Society, Washington, DC, May 1976.

[8]Chattopadhyay, A., Walsh, J. L., and Riley, M. F., "Integrated Aerodynamic Load/Dynamic Optimization of Helicopter Rotor Blades," *Journal of Aircraft*, Vol. 28, No. 1, 1991, pp. 58–65.

[9]Adelman, H. M., and Mantay, W. R., "Integrated Multidisciplinary Design Optimization of Rotorcraft," *Journal of Aircraft*, Vol. 28, No. 1, 1991, pp. 22–28.

[10]Spangler, R. L., and Hall, S. R., "Piezoelectric Actuators for Helicopter Rotor Control," *Proceedings of the 31st Structures, Structural Dynamics and Materials Conference* (Long Beach, CA), 1990, pp. 1589–1599 (AIAA Paper 90-1076).

[11]Fox, M. E., "Blade Mounted Actuation for Helicopter Rotor Control," M.S. Thesis, Massachusetts Inst. of Technology, Dept. of Aeronautics and Astronautics, Cambridge, MA, June 1993.

[12]Betz, A., "The Screw Propeller Having the Least Loss of Energy, with an Appendix by L. Prandtl," Narchrichten der Kgl. Gesellshaft der Wissenschaft, *Math.-phys Class*, Göttingen, Germany, 1919, p. 193.

[13]Prandtl, L., "Applications of Modern Hydrodynamics to Aeronautics," *Classical Aerodynamic Theory*, edited by R. T. Jones, NASA Ref. Publ. 1050, 1979; originally NACA Rept. 116, translated ca. 1921.

[14]Goldstein, S., "On the Vortex Theory of Screw Propellers," *Proceedings of the Royal Society of London*, Vol. 123, Series A, 1929, pp. 440–465.

[15]Glauert, H., "Airplane Propellers," *Aerodynamic Theory*, edited by W. F. Durand, Div. L, Vol. IV, 1935.

[16]Munro, D., private communication, Massachusetts Inst. of Technology, Cambridge, MA, 1979.

[17]Piziali, R. A., and Du Waldt, F. A., "A Method for Computing Rotary Wing Airload Distributions in Forward Flight," U.S. Army TCREC, TR 62-44, Nov. 1962.

[18]Berry, J. D., "A Multi-Element Vortex Lattice Method for Calculating the Geometry and Effects of a Helicopter Rotor Wake in Forward Flight," AIAA Paper 88-0664, Jan. 1988.

[19]Ashley, H., and Landahl, M., "Aerodynamics of Wings and Bodies," Addison-Wesley, Reading, MA, 1965, pp. 21–45.

[20]Landgrebe, A. J., and Cheney, M. C., Jr., "Rotor Wakes—Key to Performance Prediction," *Proceeding of Aerodynamics of Rotary Wings* (Marseilles, France), 1972, pp. 1-1–1-19 (AGARD 111).

[21]Larrabee, E. E., and French, S. E., "Minimum Induced Loss Windmills and Propellers," *Journal of Wind Engineering and Industrial Aerodynamics*, Vol. 15, Dec. 1983, pp. 317–327.

[22]Pierre, D. A., and Lowe, M. J., *Mathematical Programming via Augmented Lagrangians*, Addison-Wesley, Reading, MA, 1975.

[23]Johnson, W., *Helicopter Theory*, Princeton Univ. Press, Princeton, NJ, 1980.

[24]Abbot, I. H., and Von Doenhoff, A. E., *Theory of Wing Sections*, Dover, New York, 1959, p. 462.